Circumplanetary discs around young giant planets: a comparison between core-accretion and disc instability

Szulágyi, J ; Mayer, L ; Quinn, T

Abstract: Circumplanetary discs can be found around forming giant planets, regardless of whether core accretion or gravitational instability built the planet. We carried out state-of-the-art hydrodynamical simulations of the circumplanetary discs for both formation scenarios, using as similar initial conditions as possible to unveil possible intrinsic differences in the circumplanetary disc mass and temperature between the two formation mechanisms. We found that the circumplanetary discs' mass linearly scales with the circumstellar disc mass. Therefore, in an equally massive protoplanetary disc, the circumplanetary discs formed in the disc instability model can be only a factor of 8 more massive than their core-accretion counterparts. On the other hand, the bulk circumplanetary disc temperature differs by more than an order of magnitude between the two cases. The subdiscs around planets formed by gravitational instability have a characteristic temperature below 100 K, while the core-accretion circumplanetary discs are hot, with temperatures even greater than 1000 K when embedded in massive, optically thick protoplanetary discs. We explain how this difference can be understood as the natural result of the different formation mechanisms. We argue that the different temperatures should persist up to the point when a full-fledged gas giant forms via disc instability; hence, our result provides a convenient criterion for observations to distinguish between the two main formation scenarios by measuring the bulk temperature in the planet vicinity.

DOI: https://doi.org/10.1093/mnras/stw2617

Monthly Notices
of the
ROYAL ASTRONOMICAL SOCIETY

MNRAS **464,** 3158–3168 (2017)
Advance Access publication 2016 October 12

doi:10.1093/mnras/stw2617

Circumplanetary discs around young giant planets: a comparison between core-accretion and disc instability

J. Szulágyi,[1]★ L. Mayer[2] and T. Quinn[3]

[1] *ETH Zürich, Institute for Astronomy, Wolfgang-Pauli-Strasse 27, CH-8093 Zürich, Switzerland*
[2] *Center for Theoretical Astrophysics and Cosmology, Institute for Computational Science, University of Zürich, Winterthurestrasse 190, CH-8057 Zürich, Switzerland*
[3] *Astronomy Department, University of Washington, Box 351580, Seattle, WA 98195, USA*

Accepted 2016 October 10. Received 2016 October 6; in original form 2016 August 10; Editorial Decision 2016 October 6

ABSTRACT

Circumplanetary discs can be found around forming giant planets, regardless of whether core accretion or gravitational instability built the planet. We carried out state-of-the-art hydrodynamical simulations of the circumplanetary discs for both formation scenarios, using as similar initial conditions as possible to unveil possible intrinsic differences in the circumplanetary disc mass and temperature between the two formation mechanisms. We found that the circumplanetary discs' mass linearly scales with the circumstellar disc mass. Therefore, in an equally massive protoplanetary disc, the circumplanetary discs formed in the disc instability model can be only a factor of 8 more massive than their core-accretion counterparts. On the other hand, the bulk circumplanetary disc temperature differs by more than an order of magnitude between the two cases. The subdiscs around planets formed by gravitational instability have a characteristic temperature below 100 K, while the core-accretion circumplanetary discs are hot, with temperatures even greater than 1000 K when embedded in massive, optically thick protoplanetary discs. We explain how this difference can be understood as the natural result of the different formation mechanisms. We argue that the different temperatures should persist up to the point when a full-fledged gas giant forms via disc instability; hence, our result provides a convenient criterion for observations to distinguish between the two main formation scenarios by measuring the bulk temperature in the planet vicinity.

Key words: accretion, accretion discs – hydrodynamics – methods: numerical – planets and satellites: formation – planet–disc interactions.

1 INTRODUCTION

During the last stage of giant planet formation, a disc forms around the gas-giant that regulates the gas accretion on to the planet and from which the satellites form. These discs are called circumplanetary or subdiscs; the latter referring to them being embedded in the circumstellar disc. The two widely accepted planet-formation theories, core accretion (CA; Pollack et al. 1996) and gravitational instability (GI; Boss 1997), both predict that circumplanetary discs (CPDs) form around giant planets (e.g. Quillen & Trilling 1998; Canup & Ward 2002; Ward & Canup 2010).

As of yet, there is no observational evidence of a subdisc; therefore, we have to rely on numerical simulations to examine its properties. The observational efforts have just begun, e.g. with the Atacama Large Millimeter Array (Pineda et al., in preparation; Perez et al. 2015); therefore, making predictions for such observations from hydrodynamical models are crucial. Furthermore, the characteristics of the CPDs are also very important for satellite formation theory because the time-scales and the formation mechanism itself are still undetermined (e.g. Canup & Ward 2002, 2006; Mosqueira & Estrada 2003a,b).

In work so far, the masses of subdiscs formed via GI or CA have been significantly different. The GI-smoothed particle hydrodynamic (SPH) simulations of Shabram & Boley (2013) found very massive subdiscs, with 25 per cent of the planetary mass within the CPD. Similarly, Galvagni et al. (2012) and Galvagni & Mayer (2014) recovered 0.5 M_p subdiscs. Limitations of these simulations included low resolution and short-time evolution. Furthermore, they only followed the collapse of an isolated clump extracted from a global disc simulation, and therefore neglected further mass accretion and angular momentum transport from the circumstellar disc. On the other hand, CA simulations always resulted in orders of magnitude lighter CPDs (0.1–1 per cent of the planetary mass). The

★ E-mail: judit.szulagyi@phys.ethz.ch

radiative, 2D models of D'Angelo, Henning & Kley (2003) found a CPD mass of $10^{-4} M_{\rm Jup}$[1] for a Jupiter-mass planet, similar to the isothermal 3D simulations of Gressel et al. (2013). The isothermal 3D simulations of Szulágyi et al. (2014) resulted in a CPD mass of $2 \times 10^{-4} M_{\rm Jup}$ around a Jupiter-mass planet, while the radiative 3D simulations of Szulágyi (2015) found $1.5 \times 10^{-3} M_{\rm Jup}$ for the same massive gas-giant. In conclusion, simulations so far found that the GI-formed CPDs more than two orders of magnitude more massive than CA-formed subdiscs.

Regarding the temperature of the CPD, the CA and the GI simulations predict an order of magnitude difference as well. All non-isothermal CA investigations agree that the peak temperature in the inner subdisc is very high. The temperatures, of course, depend on the resolution of the simulations and on the treatment of the planetary; therefore, it is not surprising that different investigations measured somewhat different peak temperatures. For a Jupiter-mass planet, Ayliffe & Bate (2009b) argued for $T = 1600$ K at the planet surface (defined at 0.02 $R_{\rm Hill}$). They found much a higher value, $T = 4500$ K, with a realistic (i.e. smaller) planetary radius. Of course, the temperature also depends on the viscosity – through viscous heating – as was pointed out by D'Angelo et al. (2003). Their 2D radiative simulation gave a maximum of $T = 1500$ K with their highest viscosity case ($10^{16} {\rm cm}^2 {\rm s}^{-1}$) for a Jupiter-mass planet. The magneto-hydrodynamic simulations of Gressel et al. (2013) studied somewhat lower mass cores, growing the planet from 100 $M_{\rm Earth}$ to 150 $M_{\rm Earth}$, but already at these low-mass cores the temperature peaked over 1500–2000 K. Similarly, in the work of Papaloizou & Nelson (2005), the characteristic temperatures in the CPD were 1000–2000 K. The highest resolution CA simulation of Szulágyi et al. (2016a) found a maximal temperature of 13 000 K when the resolution was ∼110 000 km, i.e. 80 per cent of a Jupiter-diameter. This temperature, therefore, refers to a layer below the planetary surface of a young, puffed-up protoplanet. All the abovementioned non-isothermal CA works agreed that the temperature profile of the subdisc is very steep: from the maximal temperatures near the planet surface, it quickly declines towards the edge of the subdisc. On the other hand, the GI studies found significantly lower temperatures in the planet's vicinity. Shabram & Boley (2013) had a peak temperature of only 40 K, while Galvagni et al. (2012) obtained temperatures in the range 50–100 K in the rotationally supported envelope of the protoplanetary clump that they identified as the CPD. The latter work was able to follow the clump collapse because of two orders of magnitude higher resolution (a few Jupiter radii) and showed that the inner core of the clump heats up rapidly to temperatures higher than 1000 K, at which point dissociation of molecular hydrogen begins at the centre. In the meantime, the circumplanetary gas remained cold (<100 K). These simulations were among the first ones to show that, in GI, very soon after the collapse a clear dichotomy arises in all physical properties between an inner dense, slowly rotating core and an outer extended circumplanetary envelope or disc.

Another important difference between the CA and GI models is the mass of the circumstellar disc. The GI simulations obviously require very massive protoplanetary discs (usually ∼0.1–0.5 $M_{\rm solar}$) where GI can occur. In contrast, CA simulations use very light circumstellar discs, close to the Minimum Mass Solar Nebula estimate of ∼0.01 $M_{\rm solar}$.

The size of the protoplanet is also among the leading differences between the two formation models. In CA, the CPD formation is studied assuming that a full-fledged giant planet has already formed; therefore, approximately a Jupiter radius encloses a mass on the order of Jupiter mass. On the other hand, in the disc instability the CPD forms while the clump begins to collapse, when it has a radius as large as 2–5 au (Galvagni et al. 2012; Shabram & Boley 2013; Galvagni & Mayer 2014). This means that the gravitational potential well is much deeper in the CA simulations relative to the GI ones. As a consequence, in the former case, the accreting gas can release significantly more energy into heat compared to the second case. This can be understood due to the fact that the accretional luminosity scales inversely proportional to the accretion radius. However, this accretion radius is 1000 times larger at the onset of clump collapse than in the CA model.

An additional potentially important difference between the non-isothermal simulations of the two formation scenarios is how the thermal effects are included. The flux-limited diffusion approximation (Kley 1989; Commerçon et al. 2011) is used in a number of works on CA-formed subdiscs (e.g. Ayliffe & Bate 2009a,b; Szulágyi et al. 2016a). This method includes both radiative cooling and the heating of photons produced by the accretion luminosity. In contrast, most published GI studies (Galvagni et al. 2012; Shabram & Boley 2013; Galvagni & Mayer 2014) include a radiative cooling model designed to roughly match the radiative losses in flux-limited diffusion simulations but which neglects radiative heating via photons produced by highly compressional flows (e.g. shocks) and the effects of radiation pressure (see e.g. Boley et al. 2010, Rogers & Wadsley 2011). Some works on disc instability include flux-limited diffusion approximation, but with very low resolution (Mayer et al. 2007; Rogers & Wadsley 2011; Mayer et al. 2016).

The 1–2 orders of magnitude difference in mass and temperature would predict that observationally, the CA- and GI-formed subdiscs could be distinguished, even if the observations could only set upper limits on the CPD mass. However, these differences might come from the fact that the two sets of simulations are significantly different in the initial parameters. Motivated by these key differences, for the first time we have run simulations with very similar initial parameters (i.e. comparably massive circumstellar disc, semimajor axis, planetary mass, resolution) to unveil the real differences between GI and CA subdiscs. For the GI case, we perform the first global 3D radiative simulations with enough resolution to clearly separate the CPD and planetary core, and follow the clump collapse to relatively long time-scales in order to study how the subdisc evolves. The CA calculations are also state-of-the-art computations, as they are radiative, 3D global disc simulations with mesh refinement, which makes them one of the highest resolution studies done so far on CPDs. If the GI and CA simulations still give discrepancies in the CPD temperature and mass despite the similar initial parameters, they can provide criteria to distinguish subdiscs around CA- and GI-formed planets observationally.

2 METHODS

We use two different numerical methods to study CPDs in CA and disc instability models because the nature of the two problems is different. We used a finite-volume code that has excellent shock capturing capabilities to study CA, and a Lagrangian code that captures well the global disc dynamics and includes self-gravity, to study disc instability.

2.1 Core accretion simulations

We performed grid-based, radiative, 3D, hydrodynamic simulations with the JUPITER code (de Val-Borro et al. 2006; Szulágyi et al. 2014, 2016a; Benítez-Llambay et al. 2015; Szulágyi 2015), developed

[1] G. D'Angelo, private communications.

Table 1. Parameters of the CA hydrodynamic simulations.

	CA-1	CA-2	CA-3
CSD-mass [$M_{\rm Sol}$]	0.16	0.29	0.60
Planet-mass [$M_{\rm Jup}$]	10	10	10
Semimajor axis [au]	50	5.2	5.2

by F. Masset and J. Szulágyi. The code has nested meshes and it is based on a higher order Godunov scheme. The nested mesh technique allows having an entire circumstellar disc while zooming into the planet vicinity with higher resolution.

The radiative module includes a two-temperature approach for the flux-limited diffusion approximation (e.g. Commerçon et al. 2011). Therefore, the heating comes from adiabatic compression and viscous heating, while the cooling is through adiabatic expansion and radiation (grey-approximation). We used the gas and dust opacities of Bell & Lin (1994); therefore, despite the one-fluid (gas) simulation, the dust contribution to the temperature is taken into account. The dust-to-gas ratio was chosen to be 0.001,i.e. 10 times less than the interstellar medium value. This was motivated by the fact that at this evolutionary stage of planet formation, most of the circumstellar disc dust has already been aggregated into larger grains and planetesimals, lowering the opacity of the disc (e.g. Ormel et al. 2009, 2011). The mean molecular weight was set to 2.3, which is the solar mixture value. The equation of state is ideal gas, $P = (\gamma - 1)e$, where the adiabatic index (γ) is 1.43, P is the pressure, and e is the internal energy. We applied a low, constant kinematic viscosity of $10^{-5}{a_p}^2\Omega_p$, where a_p is the semimajor axis of the planet and Ω_p is the orbital frequency of the planet. The self-gravity of the gas is not included in these simulations.

Our simulations contain an entire circumstellar disc in the spherical coordinate system (azimuth, radius, co-latitude) centred on the one Solar-mass star. The main parameters of the simulations are in Table 1. The initial surface density profile of the circumstellar disc was flat, with zero inclination. During the first 150 orbits, we run the disc simulation without any planet in it, in order to reach initial thermal equilibrium of the disc. Then, we introduce the 10 Jupiter-mass planet through a mass-taper function, building it up continuously over 50 orbits. After this, the planet mass is kept constant throughout the simulation. The results are obtained after a steady state has been reached (175 orbits after the initial thermal equilibrium and 125 orbits after the planet was fully formed).

The nested meshes were introduced one after other, until a steady state has been reached. In these computationally expensive simulations, we have used four levels of refinement of the base mesh that contains the circumstellar disc. The refined patches include the planet vicinity, and with each level they double the resolution. On the finest level, the cell diameter was 0.000 576 854 code units, which equals to 0.002 999 64 au in the simulations where the planet was at 5.2 au, and 0.028 8427 au when the planet was placed at 50 au.

To avoid the singularity of the gravitational potential, we used the traditional epsilon-smoothing technique, where the gravitational potential is shallower within an ϵ distance from the planet:

$$U_p = -\frac{GM_p}{\sqrt{x_d^2 + y_d^2 + z_d^2 + \epsilon^2}} \quad (1)$$

where $x_d = x - x_p$, $y_d = y - y_p$, and $z_d = z - z_p$ are the distances from the planet in Cartesian coordinates, with ϵ smoothing length equal to 0.003 379 07 code units on the finest level, i.e. six cell-diameters.

More details of the JUPITER code, the simulation parameters, and the implementation can be found in Szulágyi et al. (2016a) and where similar radiative simulations were carried out on Jupiter-mass planets in low-mass circumstellar discs.

2.2 Gravitational instability simulations

In this paper, we also employ a new 3D global disc SPH simulation with unprecedented resolution, which is part of a new simulation suite to be presented in a forthcoming paper (Mayer & Quinn, in preparation). This is the first simulation that achieves a resolution of 0.01 au in a 200 au disc, comparable to the resolution of individual clump collapse local simulations (Galvagni et al. 2012). It employs as many as 42 million SPH particles. We note that the resolution is comparable to that of the CA simulations described in the previous section for the runs with the planet at large distances (52 au), which is also the configuration to be compared with the disc instability simulations.

The protoplanetary disc has a mass of $0.6 M_\odot$ and the central star is $1.35 M_\odot$, similar to the host star in the HR8799 system, the prototypical system with massive gas giants on wide orbits ($R > 30$ au) that could have been formed via disc instability. The disc temperature profile is set up in hydrostatic equilibrium using a highly accurate iterative procedure that takes into account full force balance and stellar irradiation at time $t = 0$, including disc self-gravity (Rogers & Wadsley 2011; Mayer et al. 2016). The surface density profile is a power law with an exponent close to -1 in the region where fragmentation is expected to happen ($R \sim 30$–100 au) due to shorter cooling times and low Toomre Q parameter (the minimum Toomre Q drops initially below 1.4 at $R = 60$ au), and has two exponential truncations at the inner and outer edge of the disc, which are set at 5 au and 200 au, respectively. The central star is treated as a sink particle (Rogers & Wadsley 2011), with a sink radius equal to 4 au.

The GI simulation presented in this paper was carried out with the new ChaNGa Tree+SPH code that employs a CHARM++ parallel programming environment to enable dynamic load balancing on large supercomputers (Jetley et al. 2008; Menon et al. 2015). ChaNGa inherits its basic SPH implementation from the GASOLINE and GASOLINE2 codes (Wadsley, Stadel & Quinn 2004; Keller et al. 2014; Tamburello et al. 2015), widely used in radiation hydro simulations of 3D self-gravitating discs (e.g. Mayer et al. 2002, 2007, 2016; Rogers & Wadsley 2011). As in GASOLINE2, ChaNGa employs a modern SPH implementation that uses a geometric weighting of the density estimate (Keller et al. 2014; Governato et al. 2015) resulting in a formulation of the pressure force analogous to that presented in Hopkins (2013) and Ritchie & Thomas (2001). Combined with a turbulent diffusion term in both momentum and internal energy equation – whose formulation is described in Shen, Wadsley & Stinson (2010) – and the adoption of an optional Wendland C4 kernel, it avoids artificial surface tension, resolving the mixing of different fluid phases and physical hydrodynamic instabilities at contact discontinuities. These new features have been shown to bring SPH in good agreement with finite volume grid-based codes with accurate Riemann solvers (Hopkins 2015) in modelling the properties of the flow, while keeping the advantage of a Lagrangian code in modelling disc dynamics. It provides perfect angular momentum conservation and no advection errors, which allows the capturing of processes such as ablation of clumps by ram pressure, that have never been reported before in either SPH or (fixed) grid simulations (Mayer & Quinn, in preparation).

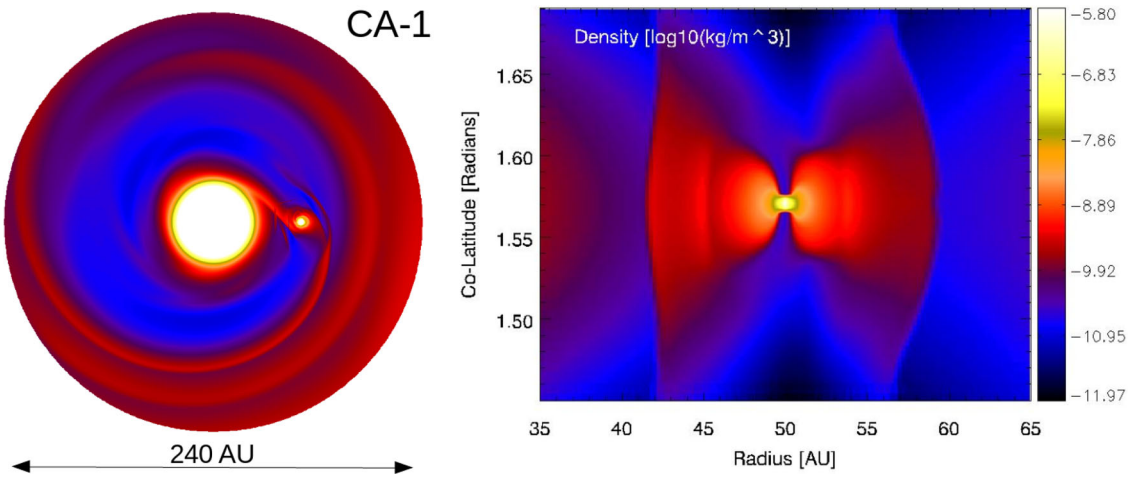

Figure 1. The CA-1 simulation, where the 10 Jupiter-mass planet is formed via CA and is placed at 50 au from the star. Left: the planet has opened a gap in the circumstellar disc. Right: zoom to the CPD through a vertical slice.

Also as in GASOLINE, ChaNGa uses a Monaghan viscosity with $\alpha = 1$ and $\beta = 2$, and a switch to limit the viscosity in purely rotational flows(Balsara 1995). The radiative cooling is based on local gas properties. For this, we write the energy loss per time per volume as

$$\Lambda = (36\pi)^{1/3}\frac{\sigma}{s}\left(T^4 - T_{\rm min}^4\right)\frac{\tau}{\tau^2+1} \qquad (2)$$

where τ represents the optical depth across a resolution element, $T_{\rm min}$ is the minimum gas background temperature (10 K), $s = (m/\rho)^{1/3}$, and σ is the Stefan–Boltzmann constant. While equation (2) is only approximate, it allows us to capture the general behaviour of radiative cooling while making the computation much faster than with full-fledged radiative transfer. Cooling is most efficient at an optical depth $\tau \sim 1$, and the two asymptotic limits for large and small τ recover the dependence of cooling rate on optical depth in the optically thin and optically thick limits. This cooling prescription compares reasonably with flux-limited diffusion calculations, as described in Boley (2009) and Boley et al. (2010). As we do not solve the radiation hydrodynamics equation in the diffusion limit, the accretional luminosity of contracting clumps is not included. However, the compressional heating – generated by PdV work – and the shock heating are taken into account.

For comparison, and in order to investigate the effect of radiation physics, we also use another version of this simulation that has 40 times lower mass resolution (gravitational softening 0.16 au) but includes mono-frequency radiative transfer (Mayer et al. 2016). This simulation of Mayer et al. (2016) was carried out with the GASOLINE code using the implicit method for flux-limited diffusion with photospheric cooling described in Rogers & Wadsley (2011), which has been shown to reproduce expected radiative losses at the disc boundary correctly, a significant improvement over previous methods of disc edge detection in SPH (e.g. Mayer et al. 2007).

In order to compute optical depths we used tabulated Rosseland mean and *Planck* opacities from D'Alessio, Calvet & Hartmann (1997) and D'Alessio, Calvet & Hartmann (2001) for the gas at solar metallicity (assuming a dust-to-gas ratio = 0.01). We included also a variable adiabatic index that takes into account the variation of the ortho/para ratio of molecular hydrogen as a function of temperature, which is important to capture the thermodynamics across spiral shocks in self-gravitating unstable discs (Podolak, Mayer & Quinn 2011). In order to speed up further the simulations during the computationally intensive phase of clump collapse, we shut off cooling in the clump core when it has collapsed to about 6 orders of magnitude higher density than the background. This essentially slows down the collapse in the inner region compared to Galvagni et al. (2012) but becomes necessary for computational reasons in order to evolve the disc for longer. We have tested that it has no effect on the CPD by running a parallel computation with no cooling shut-off.

3 RESULTS

3.1 The formation of the circumplanetary disc

In the CA simulations, the CPD forms quickly while the 10 Jupiter-mass planet is built up through the mass-tapering function (see right-hand panel of Fig. 1). Because it is not possible to follow the entire CA via hydrodynamic simulations, this initial fast planet augmentation is necessary in order to study the late stage of planet formation when a CPD forms around the gas-giant. During this phase, the subdisc is still fed by a vertical gas influx from the circumstellar disc such as described in Szulágyi et al. (2014). The planet has opened a partial, eccentric gap in the gas of the protoplanetary disc (see left-hand panel of Fig. 1).

In the GI simulation, the disc fragments into multiple clumps in the region at 60–80 au from the centre after about 500 yr, namely about one disc rotation. While a detailed description of this and other similar simulations is deferred to a forthcoming paper (Mayer & Quinn, in preparation), here, we focus on the formation of the CPDs. The clumps form with a wide range of masses, ranging between 2 and 20 Jupiter masses. Some condense out of spiral arms in relative isolation while others appear to be triggered by a strong perturbation from other clumps forming earlier (see also Armitage & Hansen 1999 and Meru 2015). The first two to three disc rotations after the onset of fragmentation mark a highly chaotic phase in which protoplanetary clumps interact vigorously among themselves and with the surrounding disc. The clumps lose mass via mutual tidal interactions and due to inward orbital migration, which in some cases appears to occur quickly, on the orbital time-scale (Malik et al. 2015), and simultaneously accrete mass from the disc. In all cases, a CPD appears at the same time as the clump formation, as the subdisc results from the higher angular momentum material accreted from the protoplanetary disc that can reach centrifugal

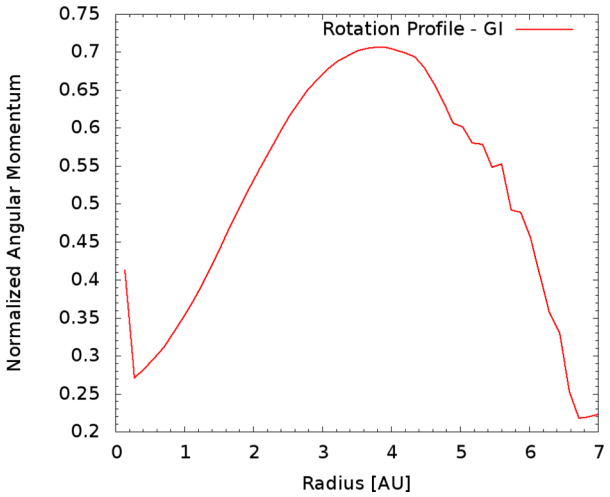

Figure 2. Normalized angular momentum (i.e. rotational velocity divided by the local Keplerian velocity) profile on the mid-plane for the GI simulation. If the normalized angular momentum is one, that means perfectly Keplerian rotation, otherwise either sub-Keplerian (<1.0) or super-Keplerian rotation (>1.0). Clearly, rotation is dynamically important in the ∼2–6 au region; this is what we will define as CPD in the following.

equilibrium around the denser core that first collapses from the spiral arm (Boley et al. 2010). The clear dichotomy between an inner dense core and an outer much more diffuse envelope, where rotation is dynamically important, can be seen on Fig. 2. Here, we show the normalized angular momentum (i.e. rotational velocity divided by the local Keplerian velocity) profile for the 10 Jupiter-mass clump soon after fragmentation. Clearly, the region between ∼2 and 6 au has the largest rotation beyond the planet, this is what we will define as CPD in the next section.

Fig. 3 shows two snapshots of the GI simulation in the early and late stage of the simulation, respectively. The second snapshot shows only four clumps remaining among those initially formed. Indeed, merger, inward migration, and tidal mass-loss are responsible for disrupting about more than half of the initially formed clumps. After 10^3 yr, the protoplanetary disc settles into a more quiet phase as its Toomre Q has risen enough to make it relatively stable. At this stage, we are left with a massive gas giant of ∼10 Jupiter masses, an larger one on the order of 20 Jupiter masses, and two even more massive objects that are clearly in the brown dwarf regime. These clumps are on eccentric orbits and have reached very high central densities at which dissociation would have already begun if included (see Section 4). Indeed, the densities are comparable to those in Galvagni et al. (2012) before the onset of dissociation, which is not included here and would not be reached anyway since we shut off the cooling in the core well before it reaches that density. Following dissociation, the core would collapse dynamically in time-scales of years to the density of Jupiter (Bodenheimer 1989; Helled, Podolak & Kovetz 2006). This 'second collapse' phase would occur below our resolution limit; hence. it cannot be followed here. It is therefore likely that these protoplanets and proto-brown dwarfs will survive indefinitely even if they migrate to less than an au from the star, although most of the CPD could be stripped in that case (see Discussion section).

The subdisc around the GI formed 10 $M_{\rm Jup}$ protoplanet has grown in mass during the interactions of the clumps, but the ratio between CPD mass and protoplanet mass has remained roughly constant, only increasing slightly (see Section 3.5). We will focus our analysis, in the rest of the paper, on the lowest mass object, the gas giant with mass around 10 Jupiter-masses; however, we also have studied the other clumps to confirm that the results presented here on the properties of the CPD are general.

3.2 Defining the circumplanetary disc boundaries

To obtain the mass of the CPD, we first need to define its boundaries. There are three main ways to define the boundary, namely:

(i) draw streamlines and account for the area where the flow is bound to the planet (i.e. orbiting around it);

(ii) compute the eccentricity of the orbit of a fluid-element at various radii from the planet, then use the circular orbits to define the boundaries; however, in case of massive planets – such as in this work – the CPD can become eccentric, so this method would not be suitable;

(iii) calculating the normalized angular momentum around the planet, meaning the z-component of the angular momentum normalized by the local Keplerian velocity at a given radius; then setting a minimum value – i.e. how sub-Keplerian the gas is in the CPD – sets the boundaries.

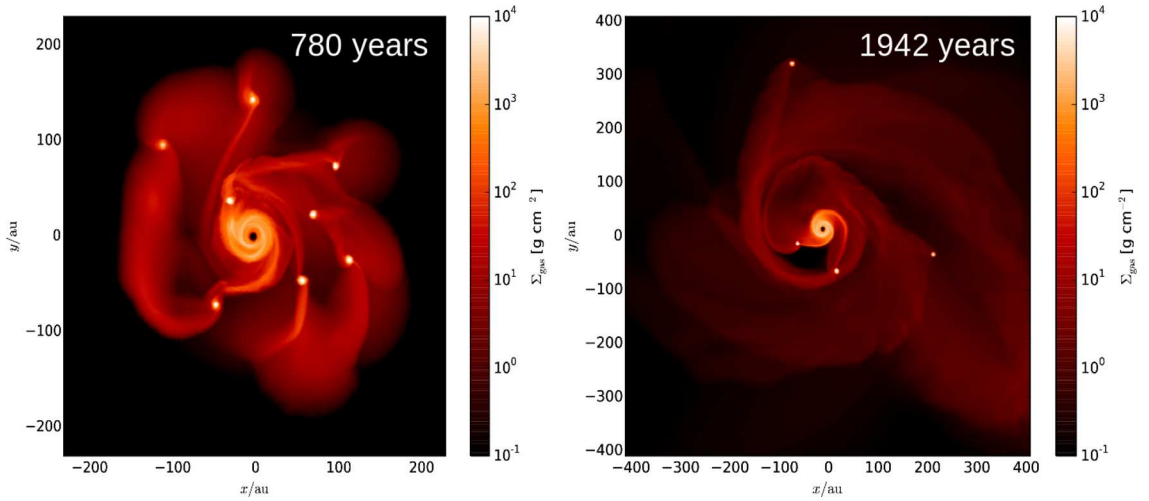

Figure 3. Two snapshots of the GI simulation at 780 yr and 1942 yr. Only four clumps survive the first chaotic interaction phase between the clumps.

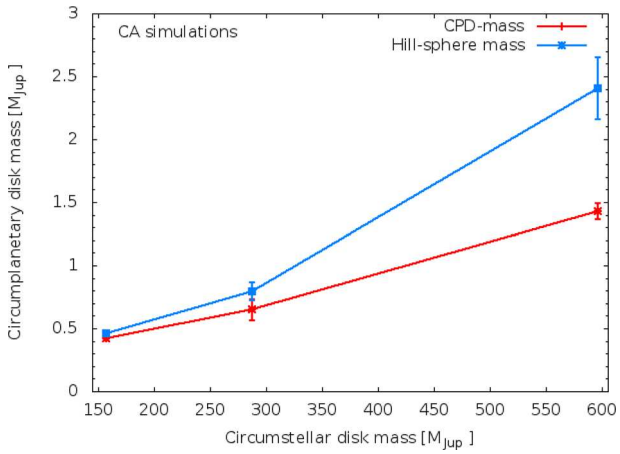

Figure 4. The CPD masses from the CA simulations as a function of the circumstellar disc masses. The CPD mass seems to scale linearly with the protoplanetary disc mass, hence even CA planets can have a very massive subdisc mass (12 per cent of the planetary mass in the case of the 600 M_{Jup} protoplanetary disc). For comparison, we also show the mass in the Hill sphere in each case; again, the relationship with the circumstellar disc mass is roughly linear.

The work of Szulágyi et al. (2014) showed that the first and third methods lead to roughly the same, 0.5 R_{Hill}, CPD radius in the case of a 1 M_J planet at 5.2 au. In this work, however, we define the CPD boundaries via the normalized angular momentum, because comparing the GI and CA simulations with this quantity is particularly useful. We decided on a 45 per cent minimum Keplerian rotation to define the boundaries of the subdiscs. Therefore the mass integral within this region – where the normalized angular momentum is larger than 0.45 – in all the different simulations can lead to a valid comparison of the CPD masses. Furthermore, we checked the streamline method, and we get roughly the same radius for the CPD as that from the >0.45 normalized angular momentum value.

Because the definition of the CPD borders is still arbitrary, we also compared the mass of the entire Hill-spheres. The CPD is definitely a subset of the Hill-sphere, and the Hill-sphere is easily definable with $R_{Hill} = a_p(M_p/M_*)^{1/3}$; therefore, the comparison of the Hill-sphere masses can eliminate any possible uncertainty of the CPD mass comparisons due to the arbitrary subdisc borders.

3.3 Comparing the density profiles and masses

As mentioned in the previous section, when calculating the masses of the CPD, we integrated the mass where the rotation of the gas is at least 45 per cent Keplerian. From the CA simulations – since all planets were 10 M_{Jup} – we compared the CPD masses with the circumstellar disc masses (see Fig. 4). The error bars were calculated as the standard deviation of 10 outputs of the simulation over one orbit of the planet. Surprisingly, even in the case of radiative simulations the CPD mass seems to (nearly) scale linearly with the circumstellar disc mass, with the relation

$$M_{CPD} = M_{CSD} \times (2.26 \pm 0.12) \times 10^{-3} + (6.49 \pm 2.37) \times 10^{-2} \quad (3)$$

This linear relationship is very important especially for observations aiming to detect the CPD because it means that the mass of the subdisc is not necessarily related to the mass of the planet, rather, more massive circumstellar discs will have more massive CPDs. Therefore, observations should not target very massive gas-giants to detect the subdisc, but instead target massive circumstellar discs where the planet has opened a gap (and therefore the gap region is optically thin).

We also compared the entire Hill-sphere masses with the circumstellar disc mass (Fig. 4). The relationship is again linear:

$$M_{Hill} = M_{CSD} \times (4.57 \pm 0.60) \times 10^{-3} - 0.37(\pm 0.24) \quad (4)$$

The Hill sphere to CPD mass ratios scale from 1.1 to 1.7 for the CA simulations, and, more massive circumstellar discs have larger mass ratios.

Because the CPD masses scale with the circumstellar disc mass, in our 0.6 M_{solar} circumstellar disc the subdisc was 1.2 M_{Jup}, giving a CPD-to-planet mass ratio of 12 per cent. This is a significantly higher ratio than found so far in CA simulations, 10^{-4}–$10^{-3} M_{planet}$ (Ayliffe & Bate 2009b; Gressel et al. 2013; Szulágyi et al. 2014, 2016a). Now it is understandable that the reason for the discrepancy is that those works all used very light circumstellar discs (∼10 M_{Jup}), so the CPD is correspondingly less massive. So far, the GI subdisc simulations predict 25 per cent M_{planet} (Shabram & Boley 2013) and 50 per cent M_{planet} (Galvagni et al. 2012). Comparing with these values from GI simulations, the CPD-to-planet mass ratios in CA simulations are lower, not by several orders of magnitude, but only by a factor of 8. Therefore, it cannot be said that GI-formed CPDs are definitely more massive; it will depend on the circumstellar disc mass. Thus, observationally, the CA and GI formation mechanisms cannot be distinguished with confidence solely from the observed CPD masses.

The subdisc masses in our GI simulations reach values even higher than the aforementioned 25–50 per cent of the planetary mass. Applying our normalized angular momentum threshold of 0.45, we find that soon after the clump forms the CPD mass is about 6 $M_{Jupiter}$ compared to 10 $M_{Jupiter}$ for the protoplanetary core inside it. At the latest time (corresponding to the snapshot on the right of Fig. 3), the subdisc grows to about 10 Jupiter-masses while the protoplanetary core, which has continued to collapse, has grown only to about 13 $M_{Jupiter}$. Hence, the CPD-to-planet ratio is roughly 60 per cent of the protoplanet mass at the beginning, in substantial agreement with the results of Galvagni et al. (2012), while at later times it becomes comparable to the protoplanet mass. We note that at late times the clump has acquired a very eccentric orbit, moving out to $R > 150$ au and gathering high angular momentum gas from the outer fringes of the disc. Accretion along this outgoing orbit might explain the increasing CPD mass with time relative to previous work. We note, in particular, that the collapsing clumps studied in Galvagni et al. (2012) were isolated hence the interplay between accretion and orbital evolution was missing by construction.

We also compared the mid-plane density profiles of the CA and the GI simulations, see Fig. 5. The CA-2 and CA-3 calculations predict larger volume densities in the mid-plane than the GI calculations, while the CA-1 simulations give the lowest density in the mid-plane. This is due to the fact that the CA simulations are more compact: the planet is a point-mass, and the CPD is not as extended as in the GI case. In the GI simulations, the planet is not a point mass, but an extended clump that is still collapsing. Fig. 5 is plotted with respect the Hill-radius, but the Hill-spheres are significantly different in physical size in the various simulations. This is the reason why the GI simulation has lower or comparable volume density in the mid-plane, but an overall more massive Hill-sphere, than in the CA simulations.

As we discuss later in the Discussion section, with increased resolution, and with the inclusion of molecular dissociation in the

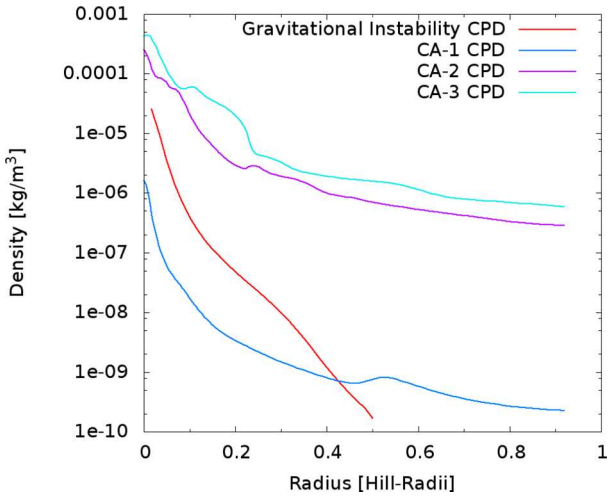

Figure 5. The mid-plane density profiles of the different simulations from the planet (left-hand side) to 1 Hill-radius. The CA-2 and CA-3 simulations have higher, and the CA-1 calculation has lower volume density in the Hill-sphere than the GI simulation.

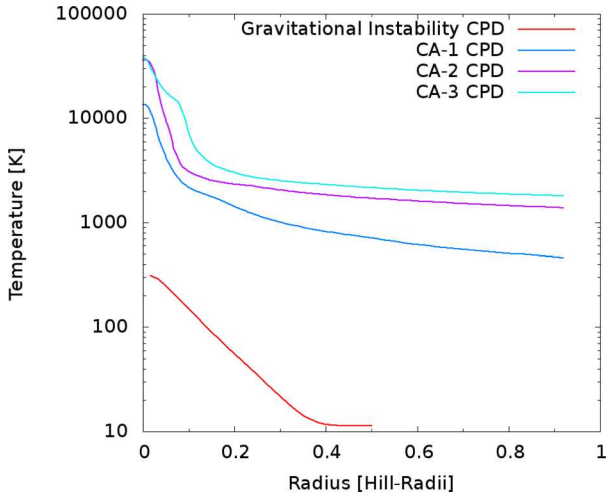

Figure 6. The mid-plane temperature profiles of the different simulations from the planet (left-hand side) to 1 Hill-radius. Clearly, all the CA simulations predict more than an order of magnitude higher temperature than the GI simulation.

GI simulations, the core is expected to collapse into a fully fledged planet of a few Jupiter radii in $<10^5$ yr (Helled et al. 2014), as hinted by the isolated collapse simulations of Galvagni et al. (2012). However, what fraction of the mass would actually collapse to this final state depends on the angular momentum profile at small radii. In Galvagni et al. (2012), the angular momentum transport from the core to the CPD was occurring due to non-axisymmetric instabilities, which appear not to be captured yet in our global simulations as we limit the cooling above a certain density. Resolving angular momentum transport processes are important in order to answer the following question; when exactly will the protoplanetary core become compact enough to be similar to the planet configuration in the CA simulations? When this happens, one would expect the CPD to evolve towards a state similar to the subdisc in the CA simulations. However, there is one aspect that will prevent the two scenarios from converging, namely the fact that the clump in the GI simulations has a significantly higher angular momentum budget. In the late stage, the total angular momentum of the subdisc in the GI simulation is about an order of magnitude higher than in the CA-1 simulation. Nevertheless, the specific angular momentum is comparable in the two cases, indicating that they are both built from material accreted from the outer circumstellar disc. The much larger CPD mass in the GI simulation ($11\,M_{\rm Jup}$ as opposed to $0.5\,M_{\rm Jup}$ in the CA-1 computation) creates a major division for the subsequent dynamical evolution. In the GI case, the protoplanetary core and the CPD will continue to collapse together, while in the CA, the subdisc will accrete on to an already compact planet.

3.4 Comparing the temperature profiles

We compared the mid-plane temperature profiles of the three CA simulations and the GI calculations inside the Hill-sphere (Fig. 6). We found more than an order of magnitude difference in the bulk temperature between the CA and the GI predictions. The latter predicts a characteristic temperature of ∼50 K in the CPD (between ∼0.1 and 0.3 Hill-radii), while the CA simulation with the planet at 50 au predicts 800–1000K inside the CPD defined in Section 3.2.

If we compare the various CA simulations with each other, we see that the Hill-sphere gas has a higher bulk temperature when the planet is at 5.2 au in contrast with the 50 au simulation. However, the difference does not come from the different semimajor axes, partially because we did not use stellar irradiation in these calculations. Instead, the difference in temperature is due to different circumstellar disc masses. In all the calculations we used a dust-to-gas ratio of 0.001; therefore, the amount of the integrated dust in the disc is also higher when the circumstellar disc mass is higher. Dust is the main heating source in protoplanetary discs, because the more dust we have, the greater the optical depth of the disc; hence, the cooling is less efficient. Even though our temperature of the CPD coincides with the drop in opacity at the dust sublimation temperature assumed in the Bell & Lin (1994) opacity table, the CPD is optically thick even across this opacity drop due to dust sublimation and the high density. If we compare the temperature profiles of this work and Szulágyi et al. (2016a) where the Jupiter-mass planet is embedded in a $\sim 10\,M_{\rm Jupiter}$ circumstellar disc, we see that the temperatures are significantly lower there.

When comparing the temperatures of two different simulations, especially with two different methodologies (here grid based and SPH computations), it is important to understand how the temperature is affected by the numerics. As we described in Section 2, the CA simulations were carried out with the flux-limited diffusion approximation, while the GI calculations were done with a phenomenological cooling law that was calibrated to flux-limited diffusion results with the same code. Another important factor for the temperature calculations is the resolution. Our hydrodynamic resolutions are comparable, the GI resolution being 10^{-2} au while the CA is 3×10^{-2} au for the planet at 50 au (simulation CA-1) and 3×10^{-3} au for the planets at 5.2 au. The gravitational softening in the GI case was 0.01 au, while it was 0.17 au for the CA-1 simulation and 0.017 au for CA-2 and CA-3. Therefore, the comparable resolutions and gravitational softenings provide valid comparisons for the temperature.

In order to check whether the lack of the flux-limited diffusion approximation in the GI simulation has an effect on the temperature, we did a comparison with a similar simulation with the flux-limited diffusion approximation included (Mayer et al. 2016) that was carried out with a similar SPH code (see Fig. 7). The clump from Mayer

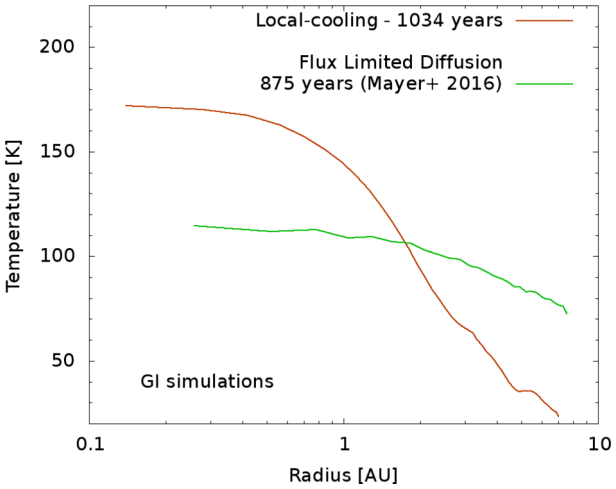

Figure 7. Comparison of the clump temperature profiles with a flux-limited diffusion simulation from (Mayer et al. 2016) (green) and this work (red) with local cooling. Clearly, the full radiative transfer with flux-limited diffusion also gives very low clump and subdisc temperatures, similar to what was found in this work. Hence, the more than an order of magnitude temperature difference found between our GI and CA simulations is robust.

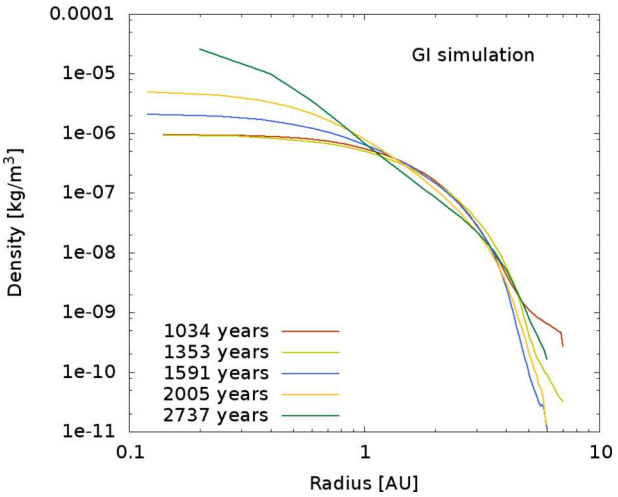

Figure 8. The time evolution of the density on the mid-plane in the GI simulation.

et al. (2016) had a mass of 8 $M_{\rm Jupiter}$, so similar to our 10 $M_{\rm Jupiter}$ protoplanet. Due to the inclusion of the flux-limited diffusion approximation in Mayer et al. (2016), the resolution is lower, and the simulation timespan is shorter than in this work. Nevertheless, as it can be seen, the comparison result is reassuring as the temperature in the outer region corresponding to the CPD is below 100 K, significantly lower than the flux-limited diffusion CA simulations.

The reason for the temperature difference between the CA and GI simulations is twofold. First, the optical depth, of course, plays a large role in determining the cooling rate. Because the CA-2 and CA-3 simulations have larger densities close to the planet than the GI calculation (see Section 3.3), the gas is more optically thick, and it cools less efficiently than in the GI case. In the GI case, optical depths are of order unity in the CPD region (but increasing to >1000 in the core), since they reflect the conditions necessary in the disc for gas to be able to fragment and form a clump, i.e. the cooling time has to be a few times the local orbital time (Gammie 2001; Rafikov 2003; Clarke & Lodato 2009). Secondly, the profile of the gravitational potential well – i.e. the size of the protoplanet – is also significantly affecting the temperature. In the GI simulations, the protoplanet has initially a size of few au before it begins to collapse. On the other hand, in the CA calculations, an entire 10 Jupiter-mass planet is compressed into a point mass with a gravitational softening of 0.17 au or 0.017 au, for planets at 50 au and 5.2 au, respectively. This means that the gravitational potential well is narrower and deeper in this case than in the GI simulations. Therefore, the gas can release more energy into heat while accreting to the planet. This can be understood with the accretional luminosity formula:

$$L_{\rm acc} = \frac{G M_p \dot{M}_p}{R_p} \tag{5}$$

where a smaller planetary radius, R_p, gives a larger accretional luminosity for the same planet mass, M_p, and the same accretion rate, $\dot{M}_p$. As we discussed in the previous section, in the GI simulation, eventually the protoplanetary core would collapse to a few Jupiter radii, which suggests the system will begin to look more like the CA case in terms of gravitational potential profile, and thus, the release of heat as gas flows inwards would also become more similar. This would imply that the CPD temperatures should become alike in the GI and CA cases. However, we pointed out in the previous section that the angular momentum budget of the planet plus CPD is significantly different in the two cases. This implies that the collapse will be different at all times. In the GI simulation, the CPD will shrink more slowly with time as angular momentum has to be removed at all radii in order for the collapse to proceed, and it may even gain angular momentum from the collapsing core due to angular momentum transport via bar-like and spiral instabilities. Galvagni et al. (2012) found that when the latter happens, the CPD becomes nearly Keplerian and reaches centrifugal equilibrium around the protoplanetary core. As a result, the CPD temperature remains low, below 100 K. While this late-stage evolution will have to be re-addressed with new, even higher resolution global simulations, it already suggests that the remarkable difference in CPD temperatures between the two formation mechanisms should persist on long time-scales, well beyond 10^4 yr.

3.5 Time-evolution of the disc instability simulations

In the case of the GI simulations, a steady state cannot be reached by the end of the simulations. A clump of a few Jupiter masses is expected to collapse into bona-fide gas giant of about a Jupiter radius in 10^4–10^5 yr, depending on the angular momentum, the metal enrichment during the collapse, the mass accretion rate from the disc, and other conditions (Helled et al. 2014). The collapse time-scale is generally defined as the time it takes to reach H_2 dissociation, which triggers a dynamical collapse. It is numerically very challenging to follow the collapse all the way with hydrodynamic simulations, partially because the more compact the clump, the slower the computation. We managed to follow the GI collapse for almost a hundred CPD dynamical times, because of access to one of the fastest supercomputer in the world. Once the inner dense core of the clump contracts to a couple of gravitational softening lengths ($\sim$0.02 au) the collapse is artificially halted in our GI simulation, but this is not an issue for studying the subdisc.

Fig. 8 shows the time evolution of the clump's density in the mid-plane between 1034 and 2736 yr. As the clump collapse to form the planet, the peak density in the centre increases, while in

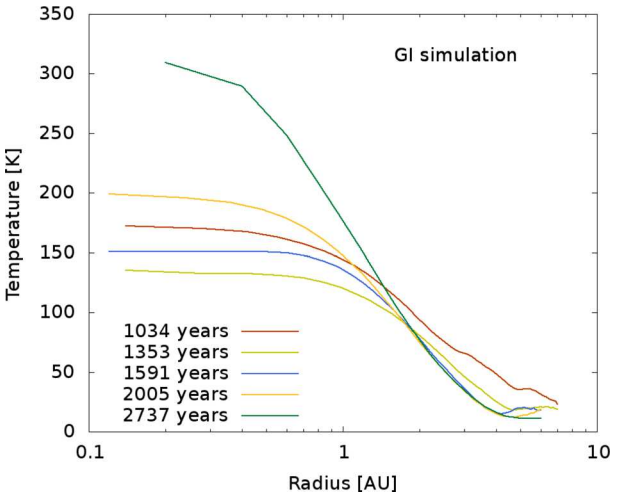

Figure 9. The mid-plane temperature profiles of the different simulations from the planet (left-hand side) to 1 Hill-radius. Clearly, all the CA simulations predict more than an order of magnitude higher temperatures than the GI simulations.

the outer parts of the clump density decreases. Understanding the time evolution of the simulation is important when comparing it with the CA simulations, where a steady state has already been reached[2].

We also show on Fig. 9 how the temperature changes during the collapse of the clump. While the temperature rises in the central parts (i.e. the interior of the protoplanet) by ∼160 K over 1700 yr, the outer parts of the clump, what we call the CPD, remain roughly at the same temperature (∼20–60K). This gives us a robust comparison of temperature with the CA simulations because the temperature remains the same in the GI CPD, irrespective of the collapse. Therefore, the fact that we cannot follow the birth of the planet – i.e. the full collapse of the clump – does not change the conclusion regarding the orders of magnitude difference in circumplanetary gas temperature between the CA and GI simulations.

4 DISCUSSION

The time-scales of CA and disc instability formation mechanisms are very different: the former takes place on 10^5–10^6 yr, while the latter is $\sim 10^4$–10^5 yr long. Therefore, our two sets of simulations describe a slightly different epoch of the circumstellar disc. Our GI simulation represents a very early stage in the circumstellar disc evolution, perhaps during the Class I phase, while the CA simulations describing an epoch when the circumstellar disc is slightly more evolved, late Class-I to mid-Class II phase.

Our results, of course, have uncertainties because of the differences between the grid-based code and the SPH code. In the former, the ionization and dissociation is not included, because its numerical implementation is stable only with specific, low-order Riemann-solvers that are not the method of choice in our code (Vaidya et al. 2015); therefore, it is possible that temperatures are overestimated. On the other hand, the GI simulation does not include flux-limited diffusion approximation radiative transfer. Nevertheless, we tested the temperature of the GI simulation by comparing it to a low-resolution flux-limited diffusion approximation simulation and confirmed that they result in a very minimal difference for the CPD temperature. In this respect, our conclusion concerning the major difference between the early stage of the CPD in the GI and CA simulation is robust.

One may wonder how our conclusion would change during the subsequent evolution in the GI case after our simulation is ended, since the collapse of the planet is continuing and a steady state was not reached. However, there is another key difference between our two sets of simulations that keeps our conclusion valid on a longer time-scale: the total angular momentum budget of the planet plus subdisc system. Indeed, as we have explained in Section 3.3, the CPD in the GI case has more than an order of magnitude higher angular momentum than the corresponding CA case. We also checked that the GI CPD, due to its large radius and low density, is Toomre stable, with $Q > 1.5$ at all times. This implies that rapid dynamical angular momentum transport via self-gravitating instabilities will not operate, but a more gentle transport can happen by global non-axisymmetric instabilities (see in Galvagni et al. 2012). The $\sim 10 M_J$ core in the GI simulation would contract to a few a Jupiter radii in $<10^5$ yr, during which time the CPD can reach centrifugal equilibrium due to internal angular momentum transport between the collapsing core and the subdisc. If the CPD is threaded by a magnetic field, it may become magneto-rotationally unstable (Fujii et al. 2014; Turner, Lee & Sano 2014), but for realistic values of viscosity ($\alpha < 0.01$), the evolutionary time-scales will be long ($>10^5$ yr). Hence we can safely conclude that the CPD by itself is a long-lasting structure despite the fact that the inner protoplanetary core has not reached a steady state and will continue to collapse further. Instead, what will likely happen is that part of the CPD could be stripped by tides if the clump plunges inwards on its eccentric orbit and reaches less than 10 au. Therefore, we predict that for GI clumps, either an extended, cold CPD is present for up to 10^5 yr, or there is no CPD if it has been lost by tides during migration. In no case do we expect a hot CPD akin to that in the CA case.

In the case of our Solar system, where the giant-planets were most likely formed via CA, the integrated mass of Jupiter's and Saturn's satellites makes up 2×10^{-4} of the planetary mass. Assuming the interstellar medium value for the dust-to-gas ratio (i.e. 1 per cent dust), this would mean a minimum mass for the CPD of 2 per cent of the masses of our two largest gas-giants. However as Canup & Ward (2002) pointed out, this mass has to be processed during the entire satellite growth time-scale, i.e. it does not all have to be present at one given instant of time. The reason is that the CPD is not a closed reservoir of mass, unlike the circumstellar disc. The subdisc is fed by the circumstellar disc, and loses mass through the accretion on to the planet. Therefore, the subdisc mass is not constant in time, but depends on the feeding and mass-loss balance, and it changes as the circumstellar disc evolves and the planet grows. Given that our Sun probably had a rather low-mass circumstellar disc, the CPDs around our gas-giants must have had low masses too. In other planetary systems, however, where the protoplanetary disc mass is higher (at present, or at earlier stage), the CPD mass can be also higher and can result in more massive, more extended satellite systems.

In the disc instability model, there might also be a second generation of subdiscs forming around the fully fledged giant planets. Indeed, if protoplanets migrate inwards to <10 au, their Hill radius will shrink; therefore, the CPDs can be stripped away by tides almost entirely (Quillen & Trilling 1998). In this case, only a dense protoplanetary core is left, which can survive even at orbital radii of ∼1 au at the densities found at the end of our GI simulation. Since

[2] Note that accretion is still ongoing in the CA simulations; therefore, the density does increase in the innermost cells around the planet point-mass.

massive protoplanets in massive self-gravitating discs can migrate inwards on time-scales of $<10^5$ yr, we argue that detection of the original CPDs formed by disc instability is more likely in the early evolutionary phase of the protoplanetary disc, before the Class II stage. Later, a new subdisc might be accreted by the newly formed gas giant, but it will be much more compact than the first population of GI subdiscs. This second generation of CPDs probably will have thermodynamic properties analogous to CA subdiscs, given that they formed around fully fledged giant planets. If such a second generation exists, then the CPDs between the two formation mechanism will not likely differ much.

5 CONCLUSION

In this paper, we compared the main characteristics (mass and temperature) of CPDs around CA, and GI-formed gas giants. We used state-of-the-art hydrodynamic simulations with as similar initial parameters as possible to reveal the key differences between the subdiscs of the two main planet formation scenarios.

The CA simulations were carried out with the JUPITER code, featuring a radiative module with the flux-limited diffusion approximation and mesh refinement. The disc instability simulations were performed with the ChaNGa SPH code, matching the resolution of the grid-based simulations and having a radiative cooling calibrated to flux-limited diffusion results. We ran three CA and one disc instability simulation with 10 Jupiter-mass planets in massive circumstellar discs (158, 290 and 600 $M_{\rm Jup}$). In two CA simulations the planets had a semimajor axis of 5.2 au, the third simulation featured a gas-giant at 50 au distance from its star. In the GI calculations, the semimajor axis was also 50 au for our chosen, 10 Jupiter-mass protoplanet, although the orbit varied a bit through interactions with other clumps.

We found from the CA simulations that the subdisc mass linearly scales with the circumstellar disc mass, even in these radiative simulations. This means that CA CPDs can be nearly as massive as their GI counterparts, if the protoplanetary disc has the same mass. In the 0.6 $M_{\rm solar}$ circumstellar discs, the CA simulation resulted in a CPD with a mass of 12 per cent $M_{\rm p}$, while we found a CPD mass of 50–100 per cent $M_{\rm p}$ in the GI computation. Previous works predicted a 4–5 orders of magnitude mass discrepancy, but we were able to show that was because of their orders of magnitude differences in circumstellar disc masses.

On the other hand, our finding is that the temperature differs by more than an order of magnitude between the GI- and CA-formed CPDs. According to the simulations, the bulk subdisc temperature is <100 K in the case of disc instability, and over 800 K for all the CA computations presented in this paper. The reason for this discrepancy lies in the different gravitational potential wells and opacities. Because the protoplanet is a few au wide extended clump in the GI simulations, while it is a fully formed giant planet with a radius of 0.17 au (meaning the gravitational potential smoothing length) in the CA-1 simulation, the accreted gas has significantly more energy to release into heat in the latter case than in the former.

The large temperature contrast between CA and GI CPDs provides a convenient tool for observations of young, embedded planets to distinguish between the two main formation mechanisms.

ACKNOWLEDGEMENTS

We thank the anonymous referee for the thoughtful review, which helped to improve the paper. JS acknowledges the support from the ETH Post-doctoral Fellowship from the Swiss Federal Institute of Technology (ETH Zürich). TQ was supported by NASA grant NNX15AE18G. This work has been in part carried out within the frame of the National Centre for Competence in Research 'PlanetS' supported by the Swiss National Science Foundation. Computations have been done on the 'Mönch' and 'Piz Dora' machines hosted at the Swiss National Computational Centre.

REFERENCES

Armitage P. J., Hansen B. M. S., 1999, Nature, 402, 633
Ayliffe B. A., Bate M. R., 2009a, MNRAS, 393, 49
Ayliffe B. A., Bate M. R., 2009b, MNRAS, 397, 657
Balsara D. S., 1995, J. Comput. Phys., 121, 357
Bell K. R., Lin D. N. C., 1994, ApJ, 427, 987
Benítez-Llambay P., Masset F., Koenigsberger G., Szulágyi J., 2015, Nature, 520, 63
Bodenheimer P., 1989, QJRAS, 30, 169
Boley A. C., 2009, ApJ, 695, L53
Boley A. C., Hayfield T., Mayer L., Durisen R. H., 2010, Icarus, 207, 509
Boss A. P., 1997, Science, 276, 1836
Canup R. M., Ward W. R., 2002, AJ, 124, 3404
Canup R. M., Ward W. R., 2006, Nature, 441, 834
Clarke C. J., Lodato G., 2009, MNRAS, 398, L6
Commerçon B., Teyssier R., Audit E., Hennebelle P., Chabrier G., 2011, A&A, 529, A35
D'Alessio P., Calvet N., Hartmann L., 1997, ApJ, 474, 397
D'Alessio P., Calvet N., Hartmann L., 2001, ApJ, 553, 321
D'Angelo G., Henning T., Kley W., 2003, ApJ, 599, 548
de Val-Borro M. et al., 2006, MNRAS, 370, 529
Fujii Y. I., Okuzumi S., Tanigawa T., Inutsuka S.-I., 2014, ApJ, 785, 101
Galvagni M., Mayer L., 2014, MNRAS, 437, 2909
Galvagni M. et al., 2012, MNRAS, 427, 1725
Gammie C. F., 2001, ApJ, 553, 174
Governato F. et al., 2015, MNRAS, 448, 792
Gressel O., Nelson R. P., Turner N. J., Ziegler U., 2013, ApJ, 779, 59
Helled R., Podolak M., Kovetz A., 2006, Icarus, 185, 64
Helled R. et al., 2014, in Beuther H., Klessen R. S., Dullemond C. P., Henning T. eds, Protostars and Planets VI. Univ. Arizona Press, Tucson, p. 643
Hopkins P. F., 2013, MNRAS, 428, 2840
Hopkins P. F., 2015, MNRAS, 450, 53
Jetley P., Gioachin F., Mendes C., Kale L., Quinn Th., 2008, Proc. IEEE Int. Parallel and Distributed Processing Symp., p. 1
Keller B. W., Wadsley J., Benincasa S. M., Couchman H. M. P., 2014, MNRAS, 442, 3013
Kley W., 1989, A&A, 208, 98
Malik M., Meru F., Mayer L., Meyer M., 2015, ApJ, 802, 56
Mayer L., Quinn T., Wadsley J., Stadel J., 2002, Science, 298, 1756
Mayer L., Lufkin G., Quinn T., Wadsley J., 2007, ApJ, 661, L77
Mayer L., Peters T., Pineda J. E., Wadsley J., Rogers P., 2016, ApJ, 823, L36
Menon H., Wesolowski L., Zheng G. et al., 2015, Comput. Astrophys. Cosmol., 2, 1
Meru F., 2015, MNRAS, 454, 2529
Mosqueira I., Estrada P. R., 2003a, Icarus, 163, 198
Mosqueira I., Estrada P. R., 2003b, Icarus, 163, 232
Ormel C. W., Paszun D., Dominik C., Tielens A. G. G. M., 2009, A&A, 502, 845
Ormel C. W., Min M., Tielens A. G. G. M., Dominik C., Paszun D., 2011, A&A, 532, A43
Papaloizou J. C. B., Nelson R. P., 2005, A&A, 433, 247
Perez S. et al., 2015, ApJ, 811, L5
Podolak M., Mayer L., Quinn T., 2011, ApJ, 734, 56
Pollack J. B. et al., 1996, Icarus, 124, 62
Quillen A. C., Trilling D. E., 1998, ApJ, 508, 707
Rafikov R. R., 2003, AJ, 126, 2529

Ritchie B. W., Thomas P. A., 2001, MNRAS, 323, 743
Rogers P. D., Wadsley J., 2011, MNRAS, 414, 913
Shabram M., Boley A. C., 2013, ApJ, 767, 63
Shen S., Wadsley J., Stinson G., 2010, MNRAS, 407, 1581
Szulágyi J., 2015, PhD thesis, Univ. Nice Sophia, Antipolis
Szulágyi J., Morbidelli A., Crida A., Masset F., 2014, ApJ, 782, 65
Szulágyi J., Masset F., Lega E., Crida A., Morbidelli A., Guillot T., 2016, MNRAS, 460, 2853
Tamburello V., Mayer L., Shen S., Wadsley J., 2015, MNRAS, 453, 2490
Turner N. J., Lee M. H., Sano T., 2014, ApJ, 783, 14
Vaidya B., Mignone A., Bodo G., Massaglia S., 2015, A&A, 580, A110
Wadsley J. W., Stadel J., Quinn T., 2004, New Astron., 9, 137
Ward W. R., Canup R. M., 2010, AJ, 140, 1168

This paper has been typeset from a TEX/LATEX file prepared by the author.